ChemCatChem

Research Article
doi.org/10.1002/cctc.202200446

Chemistry Europe
European Chemical Societies Publishing

www.chemcatchem.org

The Role of Vacancies in a Ti_2CT_x MXene-Derived Catalyst for Butane Oxidative Dehydrogenation

M. Ronda-Lloret,[a] T. K. Slot,[a] N. P. van Leest,[a] B. de Bruin,[a] W. G. Sloof,[b] E. Batyrev,[c] A. Sepúlveda-Escribano,[d] E. V. Ramos-Fernandez,[d] G. Rothenberg,[a] and N. R. Shiju*[a]

MXenes are a new family of 2D carbides or nitrides that have attracted attention due to their layered structure, tunable surface groups and high electrical conductivity. Here, we report for the first time that the Ti_2CT_x MXene catalyses the selective oxidative dehydrogenation of *n*-butane to butenes and 1,3-butadiene. This catalyst showed higher intrinsic activity compared to a commercial TiC and TiO_2 samples in terms of C_4 olefin formation rate. We propose that the stabilisation of structural vacancies and the change in composition (from a carbide to a mixed phase oxide) in the MXene causes its higher catalytic activity. These vacancies can lead to a higher concentration of unpaired electrons in the MXene-derived material, enhancing its nucleophilic properties and favouring the production of olefins.

Introduction

Lower olefins ($C_2^=$–$C_4^=$) are important building blocks in the production of petrochemicals, plastics, textiles, rubbers, solvents and coatings.[1,2] These olefins are traditionally obtained from naphtha cracking or from alkane dehydrogenation. However, these endothermic processes require high temperatures (> 550 °C).[3] Oxidative dehydrogenation (ODH) of alkanes is a promising alternative, as the addition of oxygen lowers the reaction temperature and increases catalyst stability by removing coke.[4,5] Yet controlling the selectivity of this reaction is a challenge. Especially at high alkane conversion levels, the over-oxidation to CO and CO_2 restricts the selectivity to olefins.

The performance of ODH reactions is often related to the availability of nucleophilic oxygen on the catalyst surface (also known as lattice O^{2-} species). When oxygen is activated on the catalyst surface, it tends to form anionic species (O_2^- and O_2^{2-}) that are more reactive, but often cause total butane oxidation and low olefin selectivity.[6,7] Catalysts that effectively convert electrophilic oxygen species into nucleophilic oxygen species are generally more selective to olefins.[8] Thus, catalyst design is crucial for controlling the type of surface oxygen species generated during ODH.

Different strategies, such as doping, surface modification, and changing the number of active sites and the nature of the oxygen species, were used for dehydrogenation and oxidative dehydrogenation of hydrocarbons.[9,10] For example, the promotion of ZrO_2 with other metal oxides was found to increase the number of coordinatively unsaturated Zr cations, which were identified as the active sites for propane dehydrogenation.[11] Elsewhere, the addition of electron-attracting dopants (boron oxide) in carbon nanotubes increased their propane ODH selectivity to propene as the formation of non-selective (electrophilic) oxygen species was supressed.[12] Wet chemical reduction of carbon nanotubes also decreased the concentration of electrophilic oxygen species and led to phenol group formation, increasing the selectivity to C_4 alkenes.[6]

Another way of favouring the nucleophilic character of oxygen species is by introducing structural vacancies, known as intrinsic point defects. For example, when an oxygen vacancy is introduced in the TiO_2 structure, the unpaired electrons can relocate to a titanium position (Ti^{3+}) or at the structural vacancy (forming electron-containing vacancies).[13–15] The electron-rich subsurface can make the surface oxygen species less electrophilic, which in turn enhances the selectivity to olefins during ODH.[6,16]

Here we report a novel approach in which we used the structural vacancies in a MXene material to enhance the nucleophilicity of oxygen species, thereby controlling the selectivity in butane ODH. MXenes ($M_{n+1}X_nT_x$) are a new family

[a] Dr. M. Ronda-Lloret, Dr. T. K. Slot, Dr. N. P. van Leest, Prof. Dr. B. de Bruin, Prof. Dr. G. Rothenberg, Dr. N. R. Shiju
Van 't Hoff Institute for Molecular Sciences
University of Amsterdam
Science Park 904, 1090GD Amsterdam (The Netherlands)
E-mail: n.r.shiju@uva.nl
[b] Dr. W. G. Sloof
Department of Materials Science and Engineering
Delft University of Technology
Mekelweg 2, 2628 CD Delft (The Netherlands)
[c] Dr. E. Batyrev
Tata Steel Research & Development
P.O. Box 10.000, 1970CA, IJmuiden (The Netherlands)
[d] Prof. Dr. A. Sepúlveda-Escribano, Dr. E. V. Ramos-Fernandez
Laboratorio de Materiales Avanzados, Departamento de Química Inorgánica-Instituto, Universitario de Materiales de Alicante
Universidad de Alicante
Apartado 99, E-03080 Alicante (Spain)

Supporting information for this article is available on the WWW under https://doi.org/10.1002/cctc.202200446

This publication is part of a joint Special Collection with EurJOC and EurJIC on the Netherlands Institute for Catalysis Research. Please see our homepage for more articles in the collection.

of 2D carbides or nitrides where M represents an early transition metal, X is carbon and/or nitrogen, T_x represents surface terminations such as fluorine, hydroxyl and/or oxygen atoms, and n = 1, 2 or 3.[17] MXenes (for example Ti_2CT_x) are generally obtained from the chemical etching of the respective MAX phases (in this example, Ti_2AlC), inheriting their carbon vacancy sites.[14,16,19] During chemical etching, titanium vacancies can also form in the MXene structure. Previous work found the presence of these vacancies in $Ti_3C_2T_x$ and Ti_2CT_x MXenes by means of density-functional theory (DFT) calculations, electron paramagnetic resonance (EPR) and high-angle annular dark field combined with scanning transmission electron microscopy (HAADF-STEM).[14,20,21]

Despite the catalytic potential of structural vacancies in MXenes and the increasing interest of these in electro- and photo-catalytic applications,[22,23] the use of MXene vacancy sites in thermal heterogeneous catalysis remains unexplored. Here we show that vacancy sites in MXenes can affect the catalytic performance. We tested a Ti_2CT_x MXene-derived catalyst during *n*-butane oxidative dehydrogenation (Scheme 1), which is believed to proceed via the Mars-van Krevelen mechanism.[24,25] The targeted products (by order of increasing demand) are: 1,3-butadiene (used as raw material for the production of synthetic rubbers), isobutylene (used as precursor of octane enhancers in gasoline), and linear butenes (*i.e.* 1-butene, 2-cis-butene and 2-trans-butene), which are used for producing chemicals (such as methyl ethyl ketone) and higher olefins ($C_{5+}{}^{=}$).[1,2,10]

We hypothesise that the structural vacancies in the MXene material will stabilise nucleophilic oxygen species, which are reactive and selective to butenes. Our ODH experiments show that a Ti_2CT_x MXene-based catalyst is more active and selective than commercial TiC. As both titanium carbides are oxidised under reaction, we also tested TiO_2 samples. While pure anatase or pure rutile titania samples were inactive, a mixture of anatase and rutile was active, but it showed a lower C_4 olefin formation rate than the MXene-based catalyst. We ascribe the outstanding performance of the MXene catalyst to its ability to stabilise structural vacancies, which in turn affects its electronic properties and stabilise reactive and selective nucleophilic oxygen species on its surface.

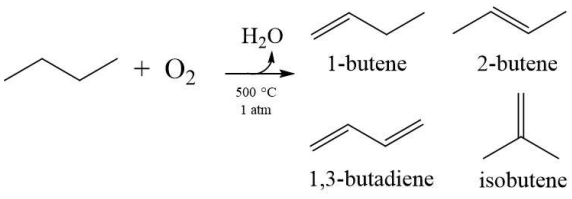

Scheme 1. C_4 olefins produced during *n*-butane oxidative dehydrogenation (ODH).

Results and Discussion

We prepared the Ti_2CT_x MXene via the chemical etching of a Ti_2AlC MAX phase (see experimental section for details). After the etching treatment (Figure 1), the characteristic (002) peaks shift to lower angles ($2\theta = 6.3°$ and 6.9°) compared to the MAX phase ($2\theta = 13°$), indicating a higher d layer spacing in the Ti_2CT_x MXene.[26] SEM analysis confirms the exfoliation of the tightly stacked layers in Ti_2AlC to Ti_2CT_x MXene accordion-like layers that give a higher BET surface area (from 1 $m^2 \cdot g^{-1}$ to 33 $m^2 \cdot g^{-1}$). Additional SEM images and the nitrogen sorption isotherms can be found in Figures S1 and S2, and Table S1.

The Ti_2CT_x MXene catalyst was active in *n*-butane ODH (see experimental section for reaction conditions). Temperature screening tests showed that the MXene is active and considerably selective to C_4 olefins from 450 °C onwards (Figure S3). The catalyst reached its highest C_4 olefin selectivity (24%) at 0.5:1 O_2/butane ratio and 500 °C (at 18% butane conversion). The produced alkenes were 2-butene (13%), 1,3-butadiene (6.0%), 1-butene (5.3%) and isobutene (0.2%). The remaining side products were CO (43%) and CO_2 (29%), which are produced from the undesired over-oxidation of butane and butenes. Trace amounts of propylene (3%) and ethane (0.5%) were also detected. We performed stability tests at 500 °C for 15 h (Figure S4). After an induction period, the conversion decreased slowly, reaching a plateau after 14 h. The catalysts were compared after reaching this stable period. A commercial TiC catalyst was less active and selective than the Ti_2CT_x MXene. Despite its similar BET surface area (TiC $S_{BET} = 27$ $m^2 \cdot g^{-1}$, Table S1) and surface composition (see Table S2), the commercial TiC showed 14% butane conversion and 11% C_4 selectivity at 0.5:1 O_2/butane ratio and 500 °C (Figure S3).

Interestingly, the Ti_2CT_x MXene is more intrinsically active than the commercial TiC (Figure 2), as it shows a higher C_4

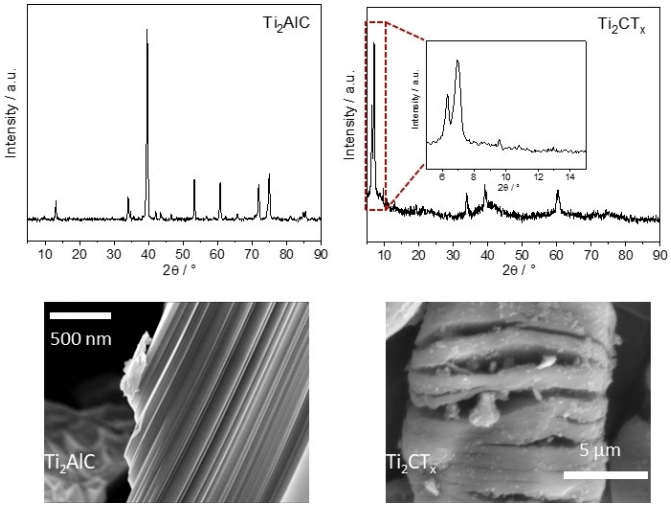

Figure 1. XRD patterns and SEM images of Ti_2AlC MAX phase and Ti_2CT_x MXene.

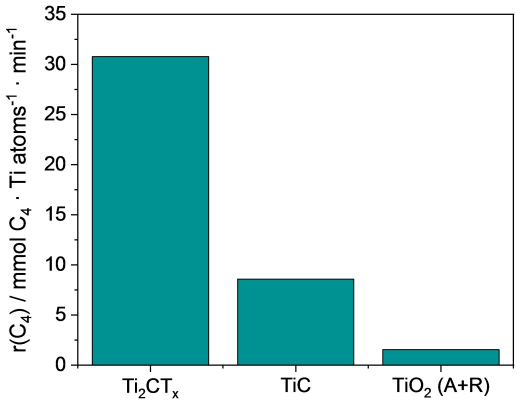

Figure 2. C_4 olefin formation rate of the studied catalysts after 0.5 h under reaction at 500 °C and O_2/butane = 1 : 1. A + R denotes anatase + rutile titania.

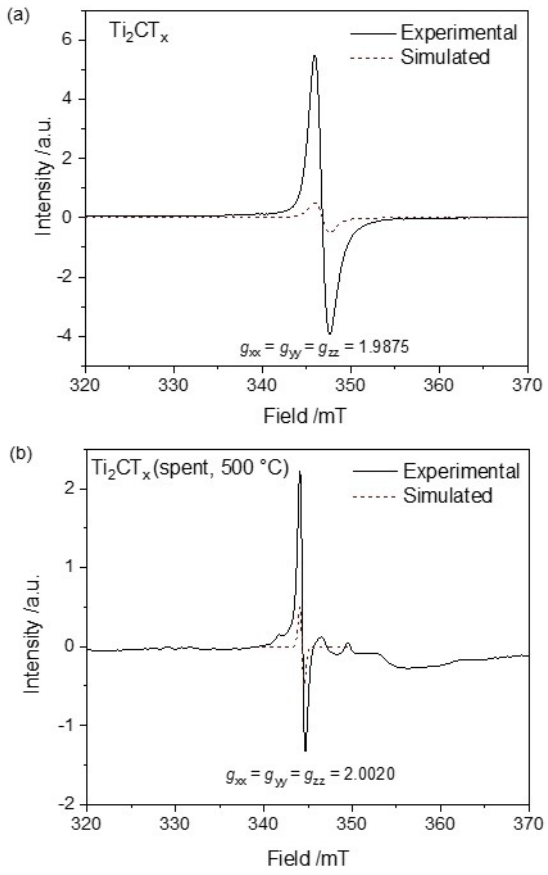

Figure 3. Experimental (measured at 10 K) and simulated EPR spectra of (a) Ti_2CT_x MXene fresh and (b) after the stability test at 500 °C. Experimental parameters; microwave frequency (a) 9.648388 GHz and (b) 9.647805, power 0.6325 mW, modulation amplitude 4.000 G.

formation rate (31 mmol $C_4 \cdot Ti\ atoms^{-1} \cdot min^{-1}$) than TiC (8.6 mmol $C_4 \cdot Ti\ atoms^{-1} \cdot min^{-1}$).

The characterisation of the as-prepared and spent catalysts gave more insights into the working of these catalysts. XPS (Figure S5) and Raman (Figure S6) show that the as-prepared Ti_2CT_x MXene contains TiO_2 (anatase and rutile) on its surface, due to its partial oxidation during synthesis.[27–36] We confirmed the presence of defects (*i.e.* unpaired electrons) in the Ti_2CT_x structure using X-band electron paramagnetic resonance (EPR). The intense featureless signal at $g_{xx} = g_{yy} = g_{zz} = 1.9875$ (Figure 3a) corresponds to Ti^{3+} regular lattice positions of the TiO_2 anatase structure and/or Ti^{3+} sites in a defective titanium carbide structure.[15,37] This reveals that the MXene contains a defective TiO_2/Ti_2CT_x structure, with oxygen and/or carbon vacancies that leave behind electrons located at Ti^{3+} positions. We believe that the MXene lattice defects promote the presence of electron-rich oxygen species that enhance the selectivity to butenes during butane ODH (previously, we showed that a similar assumption holds for the Ti_3AlC_2 MAX phase[16]).

Characterisation of the spent Ti_2CT_x and TiC materials indicate that both carbides completely oxidise to a mixture of anatase and rutile TiO_2 under reaction conditions (see XRD in Figure S7, XPS in Figure S8 and Raman in Figures S6 and S9a).[38,39] Nevertheless, the spent MXene maintains its layered structure and porosity, with only a slight decrease in the BET surface area from 33 to 26 $m^2 \cdot g^{-1}$ (see Figure S1b).

The EPR spectrum of the spent Ti_2CT_X catalyst shows a major featureless signal at $g_{xx} = g_{yy} = g_{zz} = 2.0020$ (Figure 3b), which can be attributed to oxygen centred unpaired electrons.[15,40] The spectrum shows other minor resonances, of which the small peaks located at $g < 2$ are tentatively assigned to Ti^{3+} centred unpaired electrons.[41] These results confirm that the spent MXene retains its structural vacancies.

The EPR spectrum of the spent TiC sample shows a complicated mixture of various unpaired electrons, making the definite assignment of the various components difficult (Figure S9b). The signals observed at $g > 3.5$ (< 170 mT) are indicative of inter- and intramolecular spin-spin interactions, leading to formally forbidden transitions in the X-band EPR measurement. These, combined with the observed multiple species, indicate that the unpaired electron density in spent TiC is high and distributed on different sites.

Despite their similar composition, Ti_2CT_x and commercial TiC present different electronic properties that result in different butane ODH catalytic behaviour. The spent Ti_2CT_x contains unpaired electrons mainly centred on oxygen vacancies, while the spent TiC showed a broader distribution of unpaired electrons. The electronic properties of the materials influence the type of oxygen species generated during ODH. We hypothesise that the TiC catalyst stabilises electrophilic oxygen species under reaction, favouring the over-oxidation of butane to CO and CO_2.

As both Ti_2CT_x and commercial TiC materials are oxidised to titanium oxide during the reaction, we also tested TiO_2 (anatase, rutile and a mixture of both phases) under the same conditions. Commercial anatase TiO_2 and thermally treated TiO_2 were used, and XRD and Raman spectroscopy (Figure S10) confirmed their composition. Pure anatase and pure rutile phases were inactive during *n*-butane ODH (Figure S11). This can be ascribed to the absence of defects (*i.e.* unpaired

electrons) in their structure, as the EPR spectrum of anatase TiO_2 does not show any distinct paramagnetic signal (Figure S12a). Thus, despite their high surface area, pure TiO_2 phases are not active in the reaction. The TiO_2 (A + R) catalyst was the only oxide that showed high activity, with comparable conversion values to the Ti_2CT_x catalyst (Figure S11). However, its intrinsic activity in terms of C_4 olefin formation rate was much lower compared to the Ti_2CT_x MXene (see Figure 2). This indicates that the sites on the Ti_2CT_x MXene-based catalyst are intrinsically more active despite the much lower surface Ti content (0.6 %) compared to TiO_2 (A + R) (23.4 % Ti content).

The very weak signal observed in EPR for TiO_2 (A + R) (Figure S12b) indicates only a few defects (*i.e.* oxygen vacancies). Thus, the intrinsic activity of this material is lower compared to the vacancy-rich MXene-based catalyst. Padayachee *et al.* previously reported the enhanced performance of a mixture of anatase and rutile TiO_2 phases compared to the pure individual phases during *n*-octane ODH.[8] The authors ascribed the catalytic activity to the disorder of the TiO_2 lattice at the anatase – rutile junction. This is in line with our results, as only the local disorder created in the TiO_2 (A + R) sample can convert butane into C_4 olefins. Nevertheless, the apparent lower density of unpaired electrons in this sample results in a lower C_4 formation rate compared to the MXene-based catalyst.

Overall, we show here the important role of structural defects (*i.e.* vacancies) in the electronic and catalytic properties of a MXene-derived catalyst. We believe that these properties can be explored in other type of heterogeneous catalytic applications, as already seen in dry reforming, dehydrogenation and hydrolysis reactions.[42–45] In addition, structural vacancies in MXenes are promising host sites for guest metal atoms, leading to hetero-MXenes.[46] The controlled doping of transition metals in the MXene structure broadens the scope of bifunctional catalytic systems. For example, vanadium and nitrogen groups were evenly incorporated between the $Ti_3C_2T_x$ MXene interlayers with C–V–O sites formed at the Ti vacancies.[47] Recently, Song *et al.* used Ti vacancy defects as anchoring sites for cobalt atoms, leading to a single atom Co@$Ti_{2-x}N$ material.[48]

Conclusions

This study shows the potential of structural vacancies in MXenes for heterogeneous catalysis applications. We tested a series of Ti-based materials (Ti_2CT_x MXene, commercial TiC and TiO_2) in *n*-butane oxidative dehydrogenation (ODH). The Ti_2CT_x MXene was the most active catalyst in terms of C_4 olefin formation rate. We attribute this to its final composition, a mixture of anatase and rutile TiO_2, and to its ability to stabilise structural defects. This leads to a high concentration of unpaired electrons, which favours the nucleophilic character of the catalyst surface and thus the production of olefins. A commercial TiC of similar composition was less active and selective than the MXene-based catalyst, most likely due to its electronic properties. Although the local environment of a TiO_2 (A + R) catalyst increased its activity compared to pure anatase or rutile phases, its C_4 formation rate was significantly lower compared to the MXene. We believe this is because of the low content of unpaired electrons in the (A + R) catalyst structure. Thus, the final composition of the 2D MXene-derived catalyst and the stabilisation of its vacancies, combined with its electronic properties, make MXenes promising active and stable catalysts in high-temperature reactions such as *n*-butane ODH.

Experimental Section

Materials and instrumentation

Powder X-Ray diffraction (XRD) measurements were carried out on a MiniFlex II diffractometer using Cu Kα radiation. The XRD patterns were recorded at an angle (2θ) range of 5–90° with a turning speed of $2.5^\circ \cdot min^{-1}$. N_2 adsorption-desorption isotherms at 77 K were measured on a Thermo Scientific Surfer instrument. The samples were pre-treated under vacuum at 200 °C for 16 h. X-Ray Photoelectron Spectroscopy (XPS) spectra were measured in a K-Alpha spectrometer from Thermo-Scientific. The binding energies (BE) were referenced to the C 1s line at 284.6 eV, with an accuracy of ±0.2 eV. The experimental details can be found in Ronda-Lloret *et al.*[49]

Scanning electron microscopy (SEM) micrographs were obtained on a scanning electron microscope Hitachi S3000 N. Confocal Raman spectra were recorded at 532 nm using a Renishaw (Wottonunder-Edge, United Kingdom) InVia Reflex Raman microscope with a 532 nm frequency-doubled Nd:YAG excitation source in combination with a 1800 lines mm^{-1} grating, and a Peltier-cooled CCD detector (203 K). The 521 cm^{-1} Raman shift of a silicon standard was used to verify the spectral calibration of the system.[44] X-band EPR spectra were acquired in the solid phase at 10 K on a Bruker EMX X-band spectrometer, equipped with an ER 4112HV-CF100 cryostat, and further analysed and simulated using EasySpin.[51]

Procedure for catalyst synthesis

All chemicals were obtained from commercial sources and were used as received. The synthesis of the Ti_2AlC MAX phase has been described previously.[49,50] The Ti_2CT_x MXene was prepared from the chemical etching of Ti_2AlC. In a typical procedure, 2 g of Ti_2AlC were mixed with 1.3 g of LiF previously dissolved in 100 mL of 12 M HCl. The mixture was stirred under heating at 70 °C for 24 h. The resulting powder was repeatedly centrifuged and washed with deionized water until the pH of the supernatant was neutral. The obtained solid was dried under vacuum at 30 °C for 12 h. Commercial TiC was purchased from VWR International B.V. Commercial TiO_2 anatase (Hombikat M311) was used as control sample. Rutile TiO_2 was obtained from the thermal treatment of anatase TiO_2 at 1000 °C under air for 1 h. The thermal treatment of anatase TiO_2 at 800 °C produced a mixture of anatase and rutile (A + R).

Procedure for catalytic testing

The catalysts were tested in the *n*-butane oxidative dehydrogenation (ODH) reaction using an automated six-flow parallel reactor system, which contains six quartz reactors. A total of 300 mg of catalyst was placed in the reactor in the form of pellets (1–

0.71 mm). Temperature screening tests between 400 and 600 °C were run at Ar:O_2:butane ratios of 15:0.5:1, 15:1:1 and 15:2:1. We also run stability tests for 16 h at 500 °C using a Ar:O_2:butane ratio of 15:1:1. The pressure (atmospheric) and a total flow rate of 30 mL·min^{-1} (space velocity 6000 mL·g^{-1}·h^{-1}) were kept constant. The reactants and products were detected with a GC (Interscience microGC) using flame ionization (FID) and thermal conductivity (TCD) detectors. The carbon balance remained between 98–94% at O_2:butane = 0.5:1, 98–92% at O_2:butane = 1:1, and 96–88% at O_2:butane = 2:1. C_4 alkene selectivity refers to monobutenes [1-butene, 2-butenes (cis and trans) and isobutene] and 1,3-butadiene. Propylene ($\leq$3%) and ethane (<2%) were also detected. CO and CO_2 were also detected as products of the over-oxidation of butane and butenes.

Conversion, selectivity and carbon balance values were calculated using Equations (1–3). The rate of total butenes formation (r(C_4), Eq. [4]) was calculated taking into account the amount of surface Ti available on each catalyst (based on the XPS results, Table S2) and the molecular weight of each catalyst (Mw).

$$\text{Conversion of butane } (\%) = [\text{Butane}]_{in} - [\text{Butane}]_{out/}[\text{Butane}]_{in} \cdot 100 \quad (1)$$

$$\text{Selectivity of product A } (\%) = [\text{Product A}]_{out/}[\sum \text{Products}]_{in} \cdot 100 \quad (2)$$

$$\text{Carbon balance } (\%) = [C_{out}]/[C_{in}] \cdot 100 \quad (3)$$

$$r(C_4) = \text{mmol } Bu_{in} \cdot C_4 \text{ yield})/(\%Ti_{surface} \cdot g_{catalyst} \cdot Mw_{catalyst}{}^{-1} \cdot \text{atoms Ti}) \quad (4)$$

Acknowledgements

We thank the Netherlands Organization for Scientific Research (NWO) for the grant "Developing novel catalytic materials for converting CO_2, methane and ethane to high-value chemicals in a hybrid plasma-catalytic reactor" (China.15.119). EVRF thanks the "Ministerio de Ciencia e innovación" for a grant (PID2020-116998RB-I00).

Conflict of Interest

The authors declare no conflict of interest.

Data Availability Statement

The data that support the findings of this study are available in the supplementary material of this article.

Keywords: Defects · Lower olefins · MXene · Oxygen vacancy · TiO_2

[1] H. M. Torres Galvis, K. P. de Jong, *ACS Catal.* **2013**, *3*, 2130–2149.
[2] M. Ronda-Lloret, G. Rothenberg, N. R. Shiju, *ChemSusChem* **2019**, *12*, 3896–3914.
[3] L. M. Madeira, M. F. Portela, *Catal. Rev. Sci. Eng.* **2002**, *44*, 247–286.
[4] G. Rothenberg, E. A. De Graaf, A. Bliek, *Angew. Chem. Int. Ed.* **2003**, *42*, 3365.
[5] J. T. Grant, W. P. McDermott, J. M. Venegas, S. P. Burt, J. Micka, S. P. Phivilay, C. A. Carrero, I. Hermans, *ChemCatChem* **2017**, *9*, 3623–3626.
[6] J. Li, P. Yu, J. Xie, J. Liu, Z. Wang, C. Wu, J. Rong, H. Liu, D. Su, *ACS Catal.* **2017**, *7*, 7305–7311.
[7] J. H. Blank, J. Beckers, P. F. Collignon, F. Clerc, G. Rothenberg, *Chem. Eur. J.* **2007**, *13*, 5121–5128.
[8] D. Padayachee, A. S. Mahomed, S. Singh, H. B. Friedrich, *ACS Catal.* **2020**, *10*, 2211–2220.
[9] E. A. De Graaf, G. Zwanenburg, G. Rothenberg, A. Bliek, *Org. Process Res. Dev.* **2005**, *9*, 397–403.
[10] N. Madaan, R. Haufe, N. R. Shiju, G. Rothenberg, *Top. Catal.* **2014**, *57*, 1400–1406.
[11] T. Otroshchenko, S. Sokolov, M. Stoyanova, V. A. Kondratenko, U. Rodemerck, D. Linke, E. V. Kondratenko, *Angew. Chem. Int. Ed.* **2015**, *54*, 15880–15883; *Angew. Chem.* **2015**, *127*, 16107–16111.
[12] B. Frank, J. Zhang, R. Blume, R. Schlögl, D. S. Su, *Angew. Chem. Int. Ed.* **2009**, *48*, 6913–6917; *Angew. Chem.* **2009**, *121*, 7046–7051.
[13] S. Jayashree, M. Ashokkumar, *Catalysts* **2018**, *8*, 601.
[14] T. Hu, J. Yang, X. Wang, *Phys. Chem. Chem. Phys.* **2017**, *19*, 31773–31780.
[15] M. Ivanovskaya, E. Ovodok, D. Kotsikau, I. Azarko, M. Micusik, M. Omastova, V. Golovanov, *RSC Adv.* **2020**, *10*, 25602–25608.
[16] W. H. K. Ng, E. S. Gnanakumar, E. Batyrev, S. K. Sharma, P. K. Pujari, H. F. Greer, W. Zhou, R. Sakidja, G. Rothenberg, M. W. Barsoum, et al., *Angew. Chem. Int. Ed.* **2018**, *57*, 1485–1490; *Angew. Chem.* **2018**, *130*, 1501–1506.
[17] L. Verger, V. Natu, M. Carey, M. W. Barsoum, *Trends Chem.* **2019**, *1*, 656–669.
[18] B. Anasori, M. R. Lukatskaya, Y. Gogotsi, *Nat. Rev. Mater.* **2017**, *2*, 16098.
[19] H. Zhang, T. Hu, X. Wang, Y. Zhou, *J. Mater. Sci. Technol.* **2020**, *38*, 205–220.
[20] X. Sang, Y. Xie, M. W. Lin, M. Alhabeb, K. L. Van Aken, Y. Gogotsi, P. R. C. Kent, K. Xiao, R. R. Unocic, *ACS Nano* **2016**, *10*, 9193–9200.
[21] B. Scheibe, K. Tadyszak, M. Jarek, N. Michalak, M. Kempiński, M. Lewandowski, B. Peplińska, K. Chybczyńska, *Appl. Surf. Sci.* **2019**, *479*, 216–224.
[22] H. Chen, A. D. Handoko, T. Wang, J. Qu, J. Xiao, X. Liu, D. Legut, Z. Wei Seh, Q. Zhang, *ChemSusChem* **2020**, *13*, 5690–5698.
[23] Z. Miao, G. Wang, X. Zhang, X. Dong, *Appl. Surf. Sci.* **2020**, *528*, 146929.
[24] S. Kwon, P. Deshlahra, E. Iglesia, *J. Catal.* **2018**, *364*, 228–247.
[25] J. C. Védrine, I. Fechete, *Comptes Rendus Chim.* **2016**, *19*, 1203–1225.
[26] M. Naguib, O. Mashtalir, J. Carle, V. Presser, J. Lu, L. Hultman, Y. Gogotsi, M. W. Barsoum, *ACS Nano* **2012**, *6*, 1322–1331.
[27] B. Bharti, S. Kumar, H. N. Lee, R. Kumar, *Sci. Rep.* **2016**, *6*, 32355.
[28] L. Li, G. Li, L. Tan, Y. Zhang, B. Wu, *Langmuir* **2017**, *33*, 9000–9006.
[29] B. Ahmed, D. H. Anjum, M. N. Hedhili, Y. Gogotsi, H. N. Alshareef, *Nanoscale* **2016**, *8*, 7580–7587.
[30] M. M. Ottakam Thotiyl, S. A. Freunberger, Z. Peng, Y. Chen, Z. Liu, P. G. Bruce, *Nat. Mater.* **2013**, *12*, 1050–1056.
[31] L. H. Karlsson, J. Birch, J. Halim, M. W. Barsoum, P. O. Å Persson, *Nano Lett.* **2015**, *15*, 4955–4960.
[32] J. L. Hart, K. Hantanasirisakul, A. C. Lang, B. Anasori, D. Pinto, Y. Pivak, J. T. van Omme, S. J. May, Y. Gogotsi, M. L. Taheri, *Nat. Commun.* **2019**, *10*, DOI 10.1038/s41467–018-08169–8.
[33] S. Challagulla, K. Tarafder, R. Ganesan, S. Roy, *Sci. Rep.* **2017**, *7*, 8783.
[34] V. Swamy, A. Kuznetsov, L. S. Dubrovinsky, R. A. Caruso, D. G. Shchukin, B. C. Muddle, *Phys. Rev. B: Condens. Matter Mater. Phys.* **2005**, *71*, 15–17.
[35] A. C. Ferrari, J. Robertson, *Phys. Rev. B* **2000**, *61*, 14095.
[36] M. Naguib, O. Mashtalir, M. R. Lukatskaya, B. Dyatkin, C. Zhang, V. Presser, Y. Gogotsi, M. W. Barsoum, *Chem. Commun.* **2014**, *50*, 7420–7423.
[37] A. Naldoni, M. Altomare, G. Zoppellaro, N. Liu, Š. Kment, R. Zbořil, P. Schmuki, *ACS Catal.* **2019**, *9*, 345–364.
[38] X. Liu, M. Khan, W. Liu, W. Xiang, M. Guan, P. Jiang, W. Cao, *Ceram. Int.* **2015**, *41*, 3075–3080.
[39] Y. Duan, M. Zhang, L. Wang, F. Wang, L. Yang, X. Li, C. Wang, *Appl. Catal. B* **2017**, *204*, 67–77.
[40] X. Pan, M. Q. Yang, X. Fu, N. Zhang, Y. J. Xu, *Nanoscale* **2013**, *5*, 3601–3614.
[41] L. kun Tsui, Y. Xu, D. Dawidowski, D. Cafiso, G. Zangari, *J. Mater. Chem. A* **2016**, *4*, 19070–19077.

[42] R. Thakur, A. Vahidmohammadi, J. Smith, M. Hoffman, J. Moncada, M. Beidaghi, C. A. Carrero, *ACS Catal.* **2020**, *10*, 5124–5134.
[43] J. Diao, M. Hu, Z. Lian, Z. Li, H. Zhang, F. Huang, B. Li, X. Wang, D. S. Su, H. Liu, *ACS Catal.* **2018**, *8*, 10051–10057.
[44] T. K. Slot, F. Yue, H. Xu, E. V. Ramos-Fernandez, A. Sepúlveda-Escribano, Z. Sofer, G. Rothenberg, N. R. Shiju, *2D Mater.* **2020**, *8*, 015001.
[45] Á. Morales-Garciá, F. Calle-Vallejo, F. Illas, *ACS Catal.* **2020**, *10*, 13487–13503.
[46] L. Gao, W. Bao, A. V. Kuklin, S. Mei, H. Zhang, H. Ågren, *Adv. Mater.* **2021**, 2004129.
[47] R. Cheng, Z. Wang, C. Cui, T. Hu, B. Fan, H. Wang, Y. Liang, C. Zhang, H. Zhang, X. Wang, *J. Phys. Chem. C* **2020**, *124*, 6012–6021.
[48] H. Song, R. Du, Y. Wang, D. Zu, R. Zhou, Y. Cai, F. Wang, Z. Li, Y. Shen, C. Li, *Appl. Catal. B* **2021**, *286*, 119898.
[49] M. Ronda-Lloret, V. S. Marakatti, W. G. Sloof, J. J. Delgado, A. Sepúlveda-Escribano, E. V. Ramos-Fernandez, G. Rothenberg, N. R. Shiju, *ChemSusChem* **2020**, *13*, 6401–6408.
[50] L. Boatemaa, M. Bosch, A. S. Farle, G. P. Bei, S. van der Zwaag, W. G. Sloof, *J. Am. Ceram. Soc.* **2018**, *101*, 5684–5693.
[51] S. Stoll, A. J. Schweiger, A. J. Magn, *Resonance* **2006**, *178*, 42–55. EasySpin is available free of charge at http://easyspin.org.

Manuscript received: March 31, 2022
Revised manuscript received: May 31, 2022
Accepted manuscript online: June 4, 2022
Version of record online: July 26, 2022